Am J Transl Res 2026;18(8):6956-6973
www.ajtr.org /ISSN:1943-8141/AJTR0173964

Original Article

Regulatory role of the circHIPK3/miR-125a-5p/NDUFA5 axis in diabetic retinopathy: combined analysis of single-cell and bulk transcriptomes

Zhihui Zhang, Yuanfeng Liu, Mei Bai

Xuyong Eye Hospital, Ordos 017000, Inner Mongolia, China

Received May 11, 2026; Accepted June 16, 2026; Epub August 15, 2026; Published August 30, 2026

Abstract: Objective: To explore the expression localization, functional effects, and upstream regulatory mechanism mediated by circHIPK3 (homeodomain interacting protein kinase 3)/miR-125a-5p of NDUFA5 (NADH-ubiquinone oxidoreductase 1 alpha subcomplex 5) in diabetic retinopathy (DR) by integrating public single-cell and bulk RNA-seq data with experimental validation, thereby providing a basis for investigating DR pathogenesis and identifying therapeutic targets. Methods: scRNA-seq data of DR were obtained from the GEO database, and differential expression of the key gene NDUFA5 was validated using bulk data. Human retinal microvascular endothelial cells (hRMECs) were exposed to 30 mmol/L glucose to establish a high-glucose (HG) cell model. NDUFA5 was knocked down in hRMECs. Cell viability was detected by Cell Counting Kit-8. The levels of oxidative stress indicators (malondialdehyde [MDA], superoxide dismutase [SOD], glutathione peroxidase [GSH-Px]), and inflammatory factors (tumor necrosis factor α [TNF-α], interleukin-6 [IL-6]) were measured using ELISA. Cell migration ability was detected by Transwell assay, and tube formation ability was evaluated by tube formation assay. The expression levels of circHIPK3, miR-125a-5p, and NDUFA5 in cells were detected by RT-qPCR, and the protein expression of NDUFA5 was detected by western blot. The stability of circHIPK3 was assessed by actinomycin D treatment. RNA pull-down and dual-luciferase reporter gene assays were used to verify the binding relationships between circHIPK3/NDUFA5 and miR-125a-5p. The targeting relationship between miR-125a-5p and NDUFA5 was examined by overexpressing miR-125a-5p in HG cells. Combined inhibition of circHIPK3 and miR-125a-5p in HG cells were conducted to validate the above regulatory mechanism. Male C57BL/6J mice (6-8 weeks) were intraperitoneally injected with STZ to establish a DR mouse model. NDUFA5 was inhibited using intravitreal AAV (adeno-associated virus) injection. Retinal tissues were collected for molecular detection. Results: scRNA-seq analysis revealed that NDUFA5 was specifically enriched in retinal rod cells of DR mice, forming an NDUFA5-enriched rod cell cluster (NDUFA5+RC) enriched in oxidative phosphorylation and HIF-1 signaling pathways. The VEGFA+MUC subpopulation in Müller cells was upregulated in the DR group, enriched in DR-related core pathologic pathways such as VEGF and PI3K/Akt signaling pathways, and bioinformatic prediction enhanced communication by the PTN-SDC4 ligand-receptor pair between VEGFA+MUC and NDUFA5+RC. Bulk RNA-seq validation confirmed that NDUFA5 expression was significantly upregulated in the DR group. Under HG conditions, NDUFA5 and circHIPK3 expression increased in hRMECs, while miR-125a-5p expression decreased. Knockdown of NDUFA5 or overexpression of miR-125a-5p significantly alleviated HG-induced cellular oxidative stress, inflammatory response, and abnormalities in migration and tube formation capacity. Mechanistic validation showed that circHIPK3 is stably expressed in the cytoplasm and is capable of acting as a competitive endogenous RNA (ceRNA) by sponging miR-125a-5p, which is associated with relieved targeted inhibition of NDUFA5. Animal experiments confirmed that NDUFA5 and circHIPK3 were upregulated, while miR-125a-5p was downregulated in the retinae of DR mice. NDUFA5 inhibition significantly reduced retinal vascular leakage and acellular capillary formation, and decreased oxidative stress and inflammation. Conclusion: In DR, circHIPK3 may sponge miR-125a-5p, relieving NDUFA5 inhibition and contributing to DR progression. NDUFA5 represents a potential therapeutic target for DR.

Keywords: Diabetic retinopathy, single-cell RNA sequencing, NDUFA5, miR-125a-5p, circHIPK3, ceRNA mechanism, retinal microvascular endothelial cells, oxidative stress

https://doi.org/10.62347/FPHY7794

Introduction

Diabetic retinopathy (DR) is a retinal microvascular disorder that affects nearly all diabetic patients [1]. The pathogenesis of DR is complex and involves multiple core processes, including hyperglycemia-induced retinal cellular heterogeneity, oxidative stress outbursts, inflammatory infiltration, and endothelial dysfunction [2-4]. As a highly specialized neurovascular tissue, the retina contains multiple functionally synergistic cell types, including rod cells, Müller cells, and endothelial cells. Among these, rod cells, as the most abundant photoreceptors, are closely associated with early visual impairment in DR [5, 6]; Müller cells, as the core glial support cells of the retina, exacerbate DR progression through the release of inflammatory cytokines and regulation of angiogenesis when activated or in a state of homeostatic imbalance [7, 8]. However, traditional bulk-level studies are unable to resolve the heterogeneity of different retinal cell subsets or the dynamic intercellular communication networks, leaving critical gaps in our understanding of DR pathogenesis [9].

NDUFA5, a core subunit of mitochondrial respiratory chain complex I [10], participates in the regulation of oxidative phosphorylation and energy metabolism. Its aberrant expression has been implicated in oxidative stress and inflammation in diseases such as myocardial ischemia and tumors [11, 12]. However, the expression characteristics, functional roles, and upstream regulatory mechanisms of NDUFA5 in DR remain unclear. Non-coding RNAs play critical roles in DR pathogenesis. Among them, circRNAs act as ceRNAs to sponge miRNAs, thereby relieving post-transcriptional inhibition of target genes [13]. circHIPK3, a well-studied circRNA, has been reported to regulate target gene expression through the ceRNA mechanism in various diseases, but its role and regulatory targets in DR have not been fully elucidated [14]. miR-125a-5p has been reported to participate in the regulation of oxidative stress and inflammation in diabetic complications [15-17]; however, its possible association with circHIPK3 and NDUFA5 in DR remains experimentally unverified.

The advent of scRNA-seq technology provides a powerful tool for resolving cellular heterogeneity and intercellular communication, enabling precise localization of key gene expression at the single-cell level [18]. In this study, we combined scRNA-seq and bulk RNA-seq data to characterize the expression localization of NDUFA5 in DR at the cellular subset level. Although scRNA-seq revealed NDUFA5 enrichment in rod cells, we selected hRMECs for mechanistic validation because they are key effector cells mediating retinal vascular dysfunction, leakage, and neovascularization in DR. We performed cellular experiments to verify its role in high glucose-induced cellular injury. We further explored the upstream regulatory axis of circHIPK3/miR-125a-5p/NDUFA5 and validated the therapeutic potential of targeting NDUFA5 using a DR mouse model. This study aims to provide new theoretical insight and potential targets for the in-depth understanding and precision treatment of DR.

Materials and methods

scRNA-seq data analysis

Data were obtained from the GEO database (GSE209872), containing single-cell transcriptomic data from the retinas of three DR model mice and two normal control mice. Preprocessing was performed using the Seurat v4.1.0 package. Batch effects were removed using canonical correlation analysis (CCA). Quality control criteria: nCount < 20,000, percent.mt < 25%. Highly variable genes (n = 3000) were identified using the FindVariableFeatures function in the Seurat package for subsequent analysis. After normalization with ScaleData, PCA was performed using RunPCA, and the first 20 principal components were selected for clustering. Cell clusters were identified using FindNeighbors and FindClusters, and UMAP dimensionality reduction was performed using RunUMAP. Retinal cell marker genes from CellMarker2.0 were used to identify differentially expressed genes for each cell population via the FindAllMarkers function. Rod cells and Müller cells were extracted using the Subset function, followed by re-clustering, dimensionality reduction, and marker gene analysis. GO and KEGG enrichment analysis were performed using the clusterProfile package. Intercellular communication strength and key signaling pathways were inferred using the CellChat v1.6.1 package based on ligand-receptor interaction databases.

Bulk RNA-seq analysis

Data were obtained from the GEO database (GSE60436), containing retinal transcriptomic data from six DR patients and three normal controls. Volcano plots and boxplots were generated to validate the expression differences of key molecules identified by scRNA-seq between the DR and control groups.

DR animal model construction and grouping

Male C57BL/6J mice aged 6-8 weeks were purchased from Shanghai SLAC Laboratory Animal Co., Ltd. (SYXK (Shanghai) 2022-0012). Mice were housed in separate cages at 24±1°C, 50-60% humidity, under a 12:12 light-dark cycle, with free access to food and water. All experimental procedures complied with the NIH Guide for the Care and Use of Laboratory Animals [19].

After one week of acclimatization, 24 mice were weighed and randomly divided into four groups using a random number table: Sham, DR, DR+sh-NC, and DR+sh-NDUFA5. The Sham group received intraperitoneal injections of citrate buffer (5 mL/kg) for 5 consecutive days; the DR group received 1% STZ solution (50 mg/kg) for 5 consecutive days to induce hyperglycemia, achieving diabetes diagnostic criteria. At week 4 after STZ injection, mice in the DR+sh-NC and DR+sh-NDUFA5 groups received unilateral intravitreal injections of the respective AAV (5 μL/eye, 1×10^{12} vg/mL) for 3 consecutive days. The sh-NDUFA5 AAV and its negative control AAV sh-NC were provided by Shanghai Hanheng Biotechnology Co., Ltd. At week 8 after STZ injection, mice were deeply anesthetized with isoflurane (5% for induction, 2% for maintenance, delivered through a vaporizer). After confirming the loss of pedal withdrawal reflex and absence of breathing, mice were euthanized by cervical dislocation [20]. The injected eye was collected for molecular assays (RT-qPCR, Western blot, ELISA). All quantifications were performed by blinded observers with the mouse as the statistical unit.

Cell culture and DR model establishment

Human retinal microvascular endothelial cells (hRMECs) (CP-H130, Procell, Wuhan, China) were cultured in complete hRMEC medium (CM-H130, Procell) at 37°C in 5% CO_2. Cells were incubated in 5.5 mM D-glucose medium for 48 h as the normal glucose (NG) control group, or in 30 mM D-glucose medium for 48 h to simulate a hyperglycemic environment (HG group).

Cell transfection

miR-125a-5p inhibitor, miR-125a-5p mimic, siRNAs targeting NDUFA5 (si-NDUFA5-1, si-NDUFA5-2), siRNAs targeting circHIPK3 (si-circHIPK3-1, si-circHIPK3-2), and their respective controls (inhibitor NC, mimic NC, si-NC) were purchased from Sangon Biotech (Shanghai, China). These RNAs were transfected into hRMECs using Lipofectamine 3000 transfection reagent (L3000015, Thermo Fisher, Waltham, MA, USA) according to the manufacturer's instructions. Transfection efficiency was assessed after 48 h, and subsequent experiments were performed.

CCK-8

Cells (5×10^3) were seeded into 96-well plates. After 48 h, 10 μL of CCK-8 reagent (CK04, Dojindo Laboratories, Japan) was added and incubated for 3 h. Absorbance was measured at 450 nm using a microplate reader (Bio-Rad, Hercules, CA, USA).

RT-qPCR

Total RNA was extracted using TRIzol reagent (15596018CN, Invitrogen, Carlsbad, CA, USA). Reverse transcription to obtain cDNA was performed using a reverse transcription kit (RR047A, Takara, Tokyo, Japan). For miRNA detection, a miRNA First Strand cDNA Synthesis (Tailing Reaction) kit (B532451-0020, Sangon Biotech, China) was used. qRT-PCR was performed using SYBR® Premix Ex TaqTM II (Perfect Real Time) kit (DRR081, Takara, Toyko, Japan) and a real-time PCR system (ABI 7500, ABI, Foster City, CA, USA). Primers were synthesized by Sangon Biotech (primer sequences in **Table 1**). The C_t values were recorded, and relative gene expression was calculated using the $2^{-\Delta\Delta Ct}$ method with GAPDH or U6 as internal controls.

Western blot

Proteins were extracted from tissues and cells using a protein extraction kit (BC3710, Solarbio, Beijing, China). Proteins were separated on 10% SDS-PAGE gels and transferred to PVDF

Table 1. RT-qPCR primers

Gene name	Species	Forward Primer (5'-3')	Reverse Primer (5'-3')
hsa-circHIPK3	hsa (Human)	GGATCGGCCAGTCATGTATC	ACCGCTTGGCTCTACTTTGA
hsa-HIPK3	hsa (Human)	TCAGTAGTGCTGCACCAGTG	TATGCCACTGGGATGGGAGA
hsa-miR-125a-5p	hsa (Human)	TCCCTGAGACCCTTTAAC	TTTGGCACTAGCACATT
hsa-NDUFA5	hsa (Human)	GCACCCTACTGGAGTAAGGC	ACTTGAGGCCTGATTGCACA
hsa-GAPDH	hsa (Human)	GACAGTCAGCCGCATCTTCT	GCGCCCAATACGACCAAATC
hsa-U6	hsa (Human)	CTCGCTTCGGCAGCACA	AACGCTTCACGAATTTGCGT
mmu-circHIPK3	mmu (Mouse)	GGATCGGCCAGTCATGTATC	ACCGCTTGGCTCTACTTTGA
mmu-miR-125a-5p	mmu (Mouse)	GGGTCCCTGAGACCCTTTAAC	CAGTGCGTGTCGTGGAGT
mmu-NDUFA5	mmu (Mouse)	TCTTAGGTGACTCAGGGGCA	AACATCTGGCTCCTCGTGTG
mmu-VEGFA	mmu (Mouse)	TTCGAGGAGCACTTTGGGTC	GTGGGTGGGTGTGTCTACAG
mmu-CD31	mmu (Mouse)	GTCAGAGTCTTCCTTGCCCC	CGGGTTTCTGTTTGGCCTTG
mmu-GAPDH	mmu (Mouse)	AAGGTCATCCCAGAGCTGAA	CTGCTTCACCACCTTCTTGA
mmu-U6	mmu (Mouse)	CTCGCTTCGGCAGCACA	AACGCTTCACGAATTTGCGT

membranes. Membranes were blocked with 5% skim milk and incubated with primary antibodies overnight at 4°C. After washing, membranes were incubated with goat anti-rabbit IgG secondary antibody (1:10,000, ab6721, Abcam, Cambridge, MA, USA). Protein expression was detected using ECL Western Blotting Substrate (PE0010, Thermo Fisher Scientific, Waltham, MA, USA). GAPDH was used as an internal control. Primary antibodies used: rabbit anti-NDUFA5 (1:1,000, ab241492, Abcam), rabbit anti-GAPDH (1:1,000, ab9485, Abcam).

ELISA

Mouse serum or hRMEC culture supernatants were collected. Levels of oxidative stress markers (MDA, SOD, GSH-Px) and inflammatory cytokines (TNF-α, IL-6) in serum or cell supernatants were measured by ELISA according to the manufacturer's instructions (Nanjing Jiancheng Co., China).

Transwell migration assay

Cells were collected and washed twice with pre-chilled PBS. The cell density was adjusted to 1×10^5 cells/mL in serum-free hRMEC complete medium. Transwell chambers (3421, Corning, NY, USA) were placed into 24-well plates. The lower compartment contained medium with 10% FBS, and the upper compartment contained the cell suspension. After 48 h, migrated cells were fixed with 100% formaldehyde for 30 min, stained with 0.1% crystal violet, and observed under an inverted microscope (CKX53, Olympus).

Tube formation assay

hRMECs were seeded into 24-well plates precoated with Matrigel (BD Biosciences, USA) (300 μL) and incubated for 24 h. Tube-like structures were observed under an inverted microscope. Five random fields per well were observed, and the number of tube-like structures was quantified using ImageJ software.

Nuclear-cytoplasmic fractionation for subcellular localization of circHIPK3

Cells were resuspended in hypotonic buffer A [10 mM HEPES (pH7.5), 0.5 mM DTT, 10 mM KCl, 1.5 mM $MgCl_2$] containing protease inhibitors and RNase inhibitor (N8080119, Thermo Fisher, Waltham, MA, USA). After incubation on ice for 10 min, the mixture was centrifuged at 1000×g for 10 min at 4°C. The supernatant was further centrifuged at 15000×g for 15 min to obtain the cytoplasmic fraction. The pellet was washed twice with hypotonic buffer, resuspended in hypotonic buffer B [10 mM HEPES (pH7.5), 10 mM KCl, 1.5 mM $MgCl_2$, 0.5 mM DTT, 0.5% Nonidet P-40], incubated at 4°C for 30 min with gentle rotation, and then centrifuged at 6000×g for 10 min at 4°C. The pellet was washed once with hypotonic buffer and then resuspended in RIPA buffer [50 mM Tris-HCl (pH7.5), 150 mM KCl, 1% Nonidet P-40, 0.5% sodium deoxycholate, 0.1% SDS, 1 mM EDTA pH8.0] containing protease and RNase inhibitors. After incubation at 4°C for 30 min with gentle rotation, the mixture was centrifuged at 15000×g for 20 min, and the supernatant represented the nuclear fraction.

Actinomycin D assay for circHIPK3 stability

Cells were treated with 2.5 μg/mL actinomycin D (SBR00013, Merck, Germany) for 8 h. At 0, 2, 4, 6, and 8 h, TRIzol reagent (Invitrogen) was added to collect RNA. After RNA extraction and purification, RT-qPCR was performed.

RNA pull-down

Cells were collected and lysed (1.5×10^7). Biotin-labeled miR-125a-5p probes were synthesized by Genepharm (Shanghai, China) and incubated with streptavidin-agarose magnetic beads (20349, Thermo Fisher Scientific). Cell lysates were incubated with miR-125a-5p probes or control oligonucleotide probes overnight at 4°C. RNA complexes bound to the beads were eluted with wash buffer, and the enrichment of circHIPK3 and NDUFA5 pulled down by the miR-125a-5p probe was detected by RT-qPCR.

Dual-luciferase reporter assay

Fragments of the circHIPK3 gene containing the predicted miR-125a-5p binding site (circHIPK3-WT) or the NDUFA5 3'UTR containing the binding site (NDUFA5-WT), as well as mutant versions (circHIPK3-MUT, NDUFA5-MUT) with mutated binding sites, were synthesized and cloned into pMIR reporter plasmids (AM5795, Thermo Fisher Scientific). These reporter plasmids were co-transfected into hRMECs along with mimic NC or miR-125a-5p mimic. After 48 h, cells were collected and lysed, and luciferase activity was measured using a luciferase assay kit (K801-200, Biovision, Mountain View, CA, USA).

Statistical analysis

Statistical analyses and graphing were performed using SPSS 21.0 (IBM SPSS Statistics, Chicago, IL, USA) and GraphPad Prism 8.0 (GraphPad Software Inc., San Diego, CA, USA). Measured data were expressed as mean ± standard deviation. Normality and homogeneity of variance were first tested. For data that passed normality and homogeneity tests, comparisons between two groups were performed using t-tests. Comparisons among multiple groups were performed using one-way ANOVA or two-way ANOVA, followed by Tukey's multiple comparisons test. A two-sided $P < 0.05$ was considered significant.

Results

Expression characteristics of NDUFA5 in DR retinal tissue

Clustering analysis of scRNA-seq data from GSE209872 identified nine retinal cell types (**Figure 1A**). We further performed subcluster analysis of rod cells. According to the differences in marker genes of different clusters, rod cells were divided into three phenotypes. The first was JUN+RC cells, which expressed genes related to normal rod cell function [21], with high expression of JUN that promotes rod cell differentiation and survival, as well as normal rod function-related genes including Rp1 and Cep290. The second was Actg1+RC related to rod cell development and metabolism, with high expression of Actg1, a cytoskeleton protein, and rod metabolism-related molecules such as Sik1. The third was Ndufa5+RC with an oxidative stress-related phenotype, which highly expressed the key oxidative molecule Ndufa5 as well as related molecules including Vdac2. Meanwhile, we found that Ndufa5+RC was dominant in the DR group (**Figure 1B**). GO-KEGG analysis of significantly upregulated genes in NDUFA5+RC showed enrichment in pathways related to oxidative stress, including "oxidative phosphorylation" and "HIF-1 signaling pathway", suggesting a role of this subset in DR progression through oxidative stress (**Figure 1C**).

Müller cells are the core supporting cells of the retina, and their functional imbalance is a key driver of vascular pathology and inflammation in DR. Subcluster analysis of Müller cells identified three Müller cell phenotypes, among which the VEGFA+MUC subset was markedly increased in the DR group (**Figure 1D**). GO-KEGG enrichment analysis revealed that significantly upregulated genes in VEGFA+MUC were enriched in DR core pathologic pathways such as "VEGF signaling pathway", "PI3K/Akt signaling pathway", and "Ras signaling pathway", which is consistent with the known functions of these pathways in angiogenesis and inflammation (**Figure 1E**). To dissect the intercellular communication between key subsets, CellChat analysis was performed. Bioinformatic analysis predicted an increased communication strength via the PTN-SDC4 ligand-receptor pair between VEGFA+MUC and NDUFA5+RC (**Figure 1F**). Previous studies have implicated the PTN-SDC4 pathway in inflammation [22, 23], how-

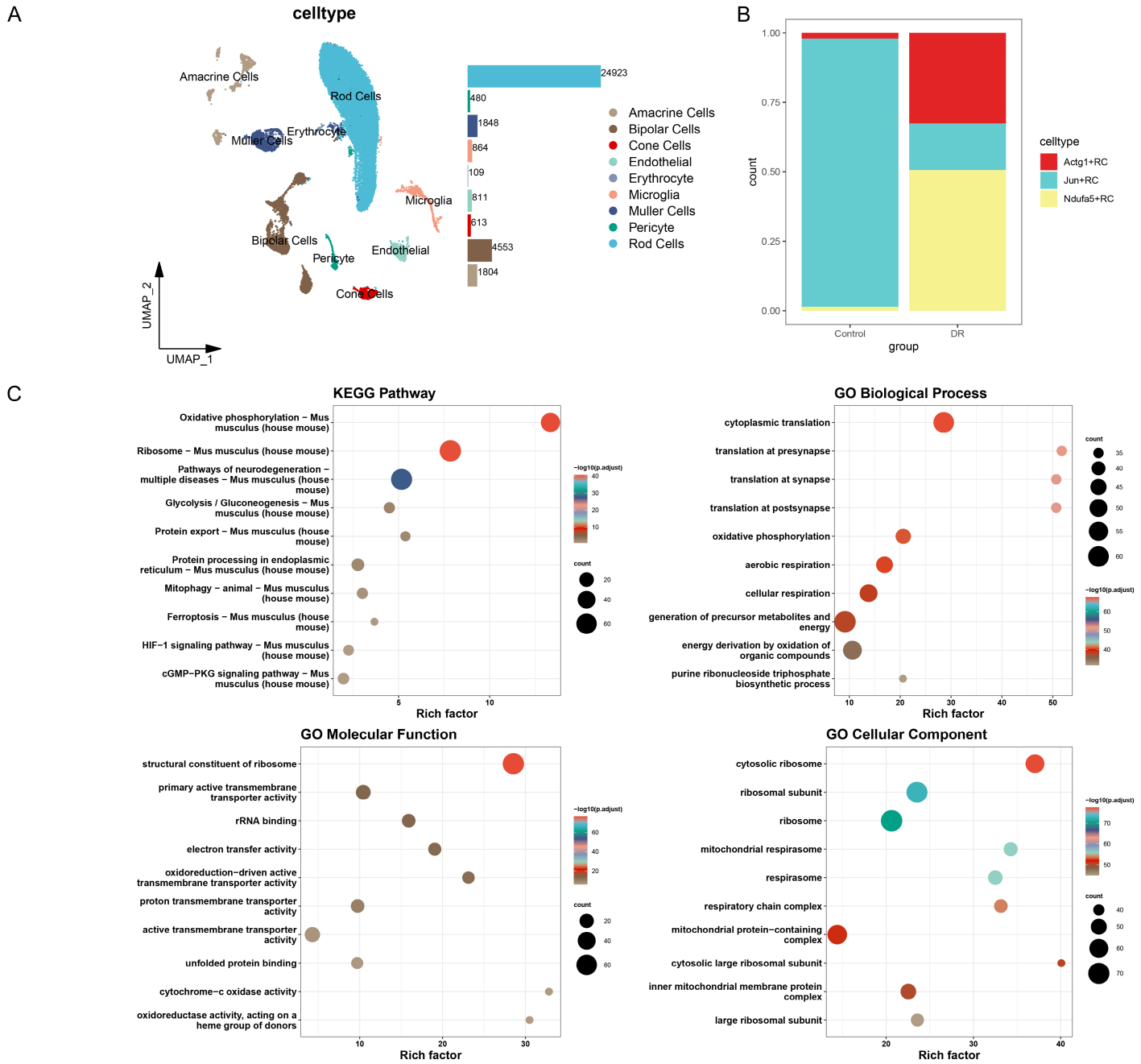
A
celltype
Amacrine Cells
Rod Cells
Erythrocyte
Muller Cells
Microglia
Bipolar Cells
Pericyte
Endothelial
Cone Cells
UMAP_2
UMAP_1
24923
480
1848
864
109
811
613
4553
1804
Amacrine Cells
Bipolar Cells
Cone Cells
Endothelial
Erythrocyte
Microglia
Muller Cells
Pericyte
Rod Cells
B
count
group
Control
DR
celltype
Actg1+RC
Jun+RC
Ndufa5+RC
C
KEGG Pathway
Oxidative phosphorylation − Mus musculus (house mouse)
Ribosome − Mus musculus (house mouse)
Pathways of neurodegeneration − multiple diseases − Mus musculus (house mouse)
Glycolysis / Gluconeogenesis − Mus musculus (house mouse)
Protein export − Mus musculus (house mouse)
Protein processing in endoplasmic reticulum − Mus musculus (house mouse)
Mitophagy − animal − Mus musculus (house mouse)
Ferroptosis − Mus musculus (house mouse)
HIF−1 signaling pathway − Mus musculus (house mouse)
cGMP−PKG signaling pathway − Mus musculus (house mouse)
Rich factor
−log10(p.adjust)
count
GO Biological Process
cytoplasmic translation
translation at presynapse
translation at synapse
translation at postsynapse
oxidative phosphorylation
aerobic respiration
cellular respiration
generation of precursor metabolites and energy
energy derivation by oxidation of organic compounds
purine ribonucleoside triphosphate biosynthetic process
Rich factor
count
−log10(p.adjust)
GO Molecular Function
structural constituent of ribosome
primary active transmembrane transporter activity
rRNA binding
electron transfer activity
oxidoreduction−driven active transmembrane transporter activity
proton transmembrane transporter activity
active transmembrane transporter activity
unfolded protein binding
cytochrome−c oxidase activity
oxidoreductase activity, acting on a heme group of donors
Rich factor
−log10(p.adjust)
count
GO Cellular Component
cytosolic ribosome
ribosomal subunit
ribosome
mitochondrial respirasome
respirasome
respiratory chain complex
mitochondrial protein−containing complex
cytosolic large ribosomal subunit
inner mitochondrial membrane protein complex
large ribosomal subunit
Rich factor
−log10(p.adjust)
count

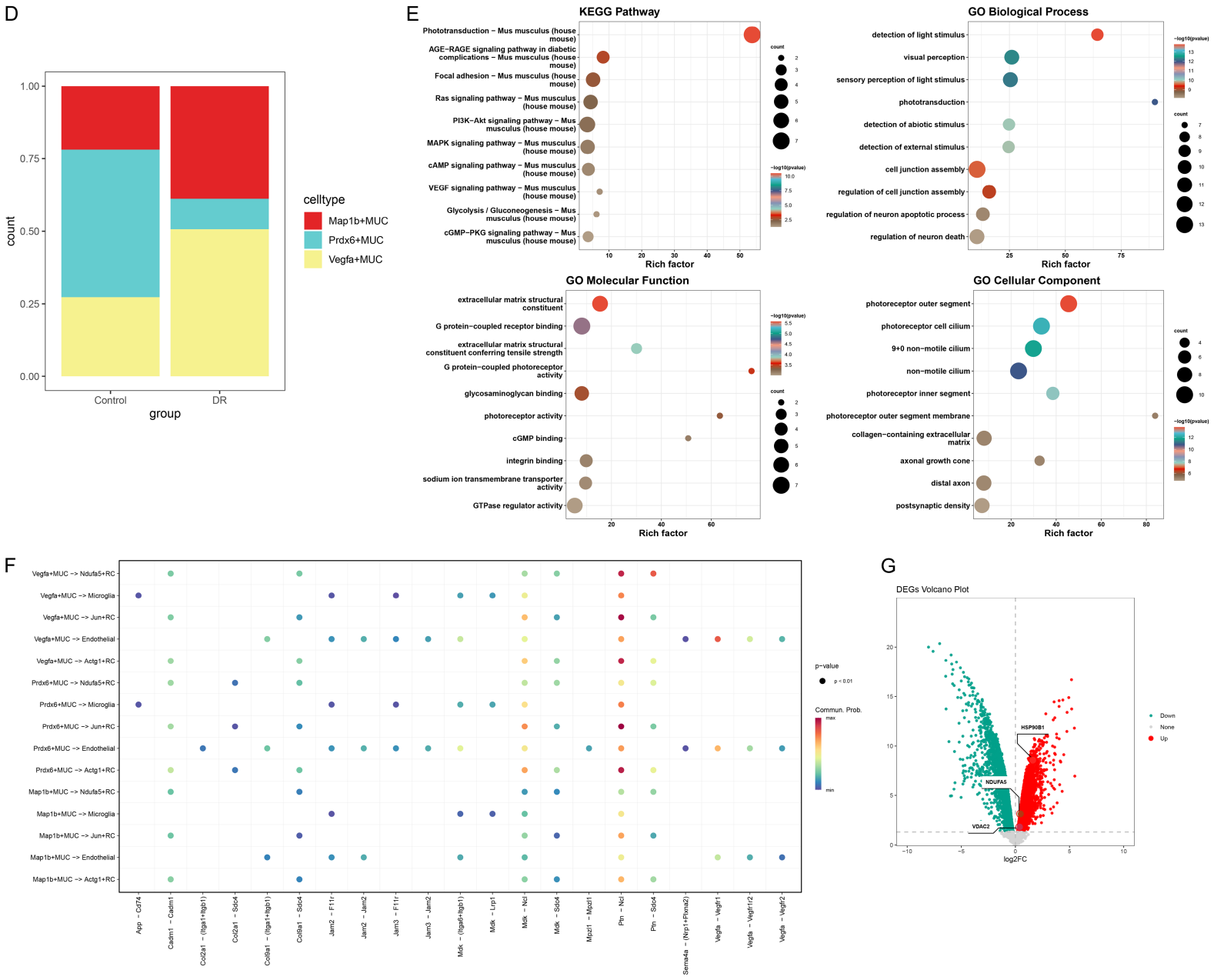
D
1.00
0.75
0.50
0.25
0.00
count
Control
DR
group
celltype
Map1b+MUC
Prdx6+MUC
Vegfa+MUC
E
KEGG Pathway
Phototransduction − Mus musculus (house mouse)
AGE−RAGE signaling pathway in diabetic complications − Mus musculus (house mouse)
Focal adhesion − Mus musculus (house mouse)
Ras signaling pathway − Mus musculus (house mouse)
PI3K−Akt signaling pathway − Mus musculus (house mouse)
MAPK signaling pathway − Mus musculus (house mouse)
cAMP signaling pathway − Mus musculus (house mouse)
VEGF signaling pathway − Mus musculus (house mouse)
Glycolysis / Gluconeogenesis − Mus musculus (house mouse)
cGMP−PKG signaling pathway − Mus musculus (house mouse)
Rich factor
GO Biological Process
detection of light stimulus
visual perception
sensory perception of light stimulus
phototransduction
detection of abiotic stimulus
detection of external stimulus
cell junction assembly
regulation of cell junction assembly
regulation of neuron apoptotic process
regulation of neuron death
Rich factor
GO Molecular Function
extracellular matrix structural constituent
G protein−coupled receptor binding
extracellular matrix structural constituent conferring tensile strength
G protein−coupled photoreceptor activity
glycosaminoglycan binding
photoreceptor activity
cGMP binding
integrin binding
sodium ion transmembrane transporter activity
GTPase regulator activity
Rich factor
GO Cellular Component
photoreceptor outer segment
photoreceptor cell cilium
9+0 non−motile cilium
non−motile cilium
photoreceptor inner segment
photoreceptor outer segment membrane
collagen−containing extracellular matrix
axonal growth cone
distal axon
postsynaptic density
Rich factor
F
Vegfa+MUC −> Ndufa5+RC
Vegfa+MUC −> Microglia
Vegfa+MUC −> Jun+RC
Vegfa+MUC −> Endothelial
Vegfa+MUC −> Actg1+RC
Prdx6+MUC −> Ndufa5+RC
Prdx6+MUC −> Microglia
Prdx6+MUC −> Jun+RC
Prdx6+MUC −> Endothelial
Prdx6+MUC −> Actg1+RC
Map1b+MUC −> Ndufa5+RC
Map1b+MUC −> Microglia
Map1b+MUC −> Jun+RC
Map1b+MUC −> Endothelial
Map1b+MUC −> Actg1+RC
App − Cd74
Cadm1 − Cadm1
Col2a1 − (Itga1+Itgb1)
Col2a1 − Sdc4
Col9a1 − (Itga1+Itgb1)
Col9a1 − Sdc4
Jam2 − F11r
Jam2 − Jam2
Jam3 − F11r
Jam3 − Jam2
Mdk − (Itga6+Itgb1)
Mdk − Lrp1
Mdk − Ncl
Mdk − Sdc4
Mpzl1 − Mpzl1
Ptn − Ncl
Ptn − Sdc4
Sema4a − (Nrp1+Plxna2)
Vegfa − Vegfr1
Vegfa − Vegfr1r2
Vegfa − Vegfr2
p−value
p < 0.01
Commun. Prob.
max
min
G
DEGs Volcano Plot
HSP90B1
NDUFA5
VDAC2
log2FC
Down
None
Up

Figure 1. Expression characteristics of NDUFA5 in DR retinal tissue. A: Retinal cell types; B: Rod cell subcluster analysis; C: GO-KEGG analysis of significantly upregulated genes in NDUFA5+RC; D: Müller cell subcluster analysis; E: GO-KEGG analysis of significantly upregulated genes in VEGFA+MUC; F: Predicted cell-cell communication based on ligand-receptor expression; G: Volcano plot of differential genes from bulk data.

ever, the functional relevance of this predicted interaction requires experimental validation. Validation using the GSE60436 bulk dataset showed that NDUFA5, HSP90B1 (oxidative stress-related), VDAC2 (mitochondrial function-related), and other genes were significantly upregulated in the DR group (**Figure 1G**), consistent with the scRNA-seq results.

NDUFA5 knockdown inhibits high glucose-induced cellular injury

To investigate the role of NDUFA5 in DR, we knocked down NDUFA5 expression in hRMECs ($P < 0.05$, **Figure 2A**) and selected si-NDUFA5-1, which showed better transfection efficiency, for subsequent experiments. HG model was established by treating with 30 mM glucose. Compared to the NG (normal glucose control), HG cells showed significantly increased viability ($P < 0.05$, **Figure 2B**), increased migration capacity ($P < 0.05$, **Figure 2C**), increased tube formation ($P < 0.05$, **Figure 2D**), elevated MDA level, decreased SOD and GSH-Px levels ($P < 0.05$, **Figure 2E-G**), and elevated TNF-α and IL-6 levels ($P < 0.05$, **Figure 2H**, **2I**), indicating that the high glucose environment induced oxidative stress and inflammation, leading to cellular injury. HG upregulated NDUFA5 expression ($P < 0.05$, **Figure 2J**, **2K**). NDUFA5 knockdown decreased cell viability, migration capacity, and tube formation ($P < 0.05$, **Figure 2B-D**), decreased MDA level, increased SOD and GSH-Px levels ($P < 0.05$, **Figure 2E-G**), and decreased TNF-α and IL-6 levels ($P < 0.05$, **Figure 2H**, **2I**). These results indicate that NDUFA5 knockdown effectively alleviates high glucose-induced oxidative stress and inflammation, thereby mitigating cellular injury.

miR-125a-5p is downregulated in DR and targets NDUFA5

To identify upstream regulators of NDUFA5, the starBase database was used to predict miRNAs targeting NDUFA5. A conserved miR-125a-5p recognition site was found in the NDUFA5 3'UTR. Previous reports have shown that overexpression of miR-125a-5p significantly reduces vascular leakage in DR [15]. Therefore, we hypothesized that miR-125a-5p might target NDUFA5 to ameliorate high glucose-induced cellular injury in DR. First, RNA pull-down and dual-luciferase reporter assays validated the binding between miR-125a-5p and NDUFA5 ($P < 0.05$, **Figure 3A**, **3B**). miR-125a-5p expression was downregulated in HG cells ($P < 0.05$, **Figure 3C**). To further confirm the targeting relationship, we overexpressed miR-125a-5p in hRMECs ($P < 0.05$, **Figure 3D**), which led to a significant decrease in NDUFA5 expression ($P < 0.05$, **Figure 3E**, **3F**). These results indicate that miR-125a-5p targets and inhibits NDUFA5 expression.

miR-125a-5p overexpression alleviates high glucose-induced retinal endothelial cell injury

To investigate the role of miR-125a-5p in HG cells, we overexpressed miR-125a-5p in HG cells ($P < 0.05$, **Figure 4A**). miR-125a-5p overexpression led to downregulation of NDUFA5 ($P < 0.05$, **Figure 4B**, **4C**), decreased cell viability, migration capacity, and tube formation ($P < 0.05$, **Figure 4D-F**), decreased MDA level, increased SOD and GSH-Px levels ($P < 0.05$, **Figure 4G-I**), and decreased TNF-α and IL-6 levels ($P < 0.05$, **Figure 4J**, **4K**). These results indicate that miR-125a-5p overexpression effectively alleviated high glucose-induced oxidative stress and inflammation, thereby mitigating cellular injury.

circHIPK3 is upregulated in HG cells and targets miR-125a-5p

The starBase database predicted binding between circHIPK3 and miR-125a-5p, and circHIPK3 has been reported to function as a miRNA sponge in DR [14, 24]. Therefore, we hypothesized that circHIPK3 targets miR-125a-5p. hRMECs were treated with actinomycin D to assess the half-life of circHIPK3. Compared with linear HIPK3, circHIPK3 exhibited greater stability, whereas linear HIPK3 was readily degraded ($P < 0.05$, **Figure 5A**). Nuclear-cytoplasmic fractionation showed that circHIPK3 was predominantly localized in the cytoplasm of hRMECs (**Figure 5B**). RNA pull-down and dual-luciferase reporter assays both con-

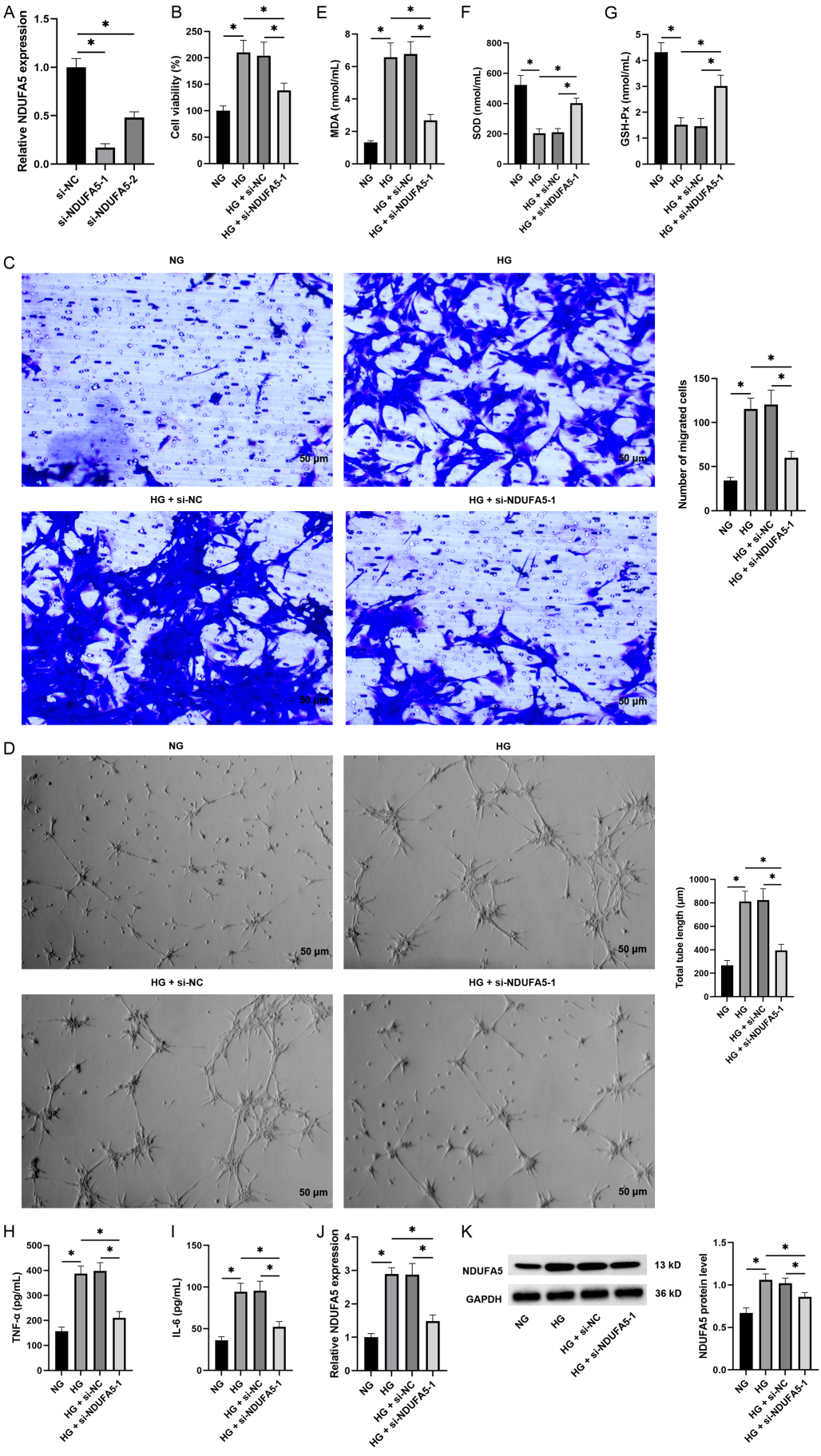
A
Relative NDUFA5 expression
si-NC
si-NDUFA5-1
si-NDUFA5-2
B
Cell viability (%)
E
MDA (nmol/mL)
F
SOD (nmol/mL)
G
GSH-Px (nmol/mL)
NG
HG
HG + si-NC
HG + si-NDUFA5-1
C
50 μm
Number of migrated cells
D
Total tube length (μm)
H
TNF-α (pg/mL)
I
IL-6 (pg/mL)
J
Relative NDUFA5 expression
K
NDUFA5
GAPDH
13 kD
36 kD
NDUFA5 protein level

Figure 2. NDUFA5 knockdown effectively alleviates high glucose-induced cellular injury. HG group: 30 mM D-glucose; NG control: 5.5 mM D-glucose. hRMECs were transfected with two siRNAs targeting NDUFA5 (si-NDUFA5-1, si-NDUFA5-2), with si-NC as control. A: RT-qPCR detection of transfection efficiency; si-NDUFA5-1 was selected for subsequent experiments. B: CCK-8 assay for cell viability. C: Transwell assay for cell migration (Scale bar = 50 μm; ×200). D: Tube formation assay for tube formation capacity (Scale bar = 50 μm; ×200). E-I: ELISA detection of oxidative stress markers (MDA, SOD, GSH-Px) and inflammatory cytokines (TNF-α, IL-6). J, K: RT-qPCR and western blot detection of NDUFA5 expression. Three independent replicates; data are mean ± SD. A-K: one-way ANOVA with Tukey's multiple comparisons test. * indicates $P < 0.05$.

firmed binding between circHIPK3 and miR-125a-5p ($P < 0.05$, **Figure 5C**, **5D**). Moreover, circHIPK3 expression was significantly increased in HG cells ($P < 0.05$, **Figure 5E**). We then knocked down circHIPK3 in hRMECs ($P < 0.05$, **Figure 5F**). circHIPK3 knockdown significantly increased miR-125a-5p expression ($P < 0.05$, **Figure 5G**) and decreased NDUFA5 expression ($P < 0.05$, **Figure 5H**, **5I**). These results indicate that circHIPK3 acts as a molecular sponge for miR-125a-5p, inhibiting miR-125a-5p expression and thereby promoting NDUFA5 expression.

circHIPK3 knockdown alleviates high glucose-induced cellular injury by upregulating miR-125a-5p

To validate the above mechanism, we knocked down circHIPK3 in HG cells ($P < 0.05$, **Figure 6A**). circHIPK3 knockdown significantly increased miR-125a-5p expression ($P < 0.05$, **Figure 6C**) and decreased NDUFA5 expression ($P < 0.05$, **Figure 6D**, **6E**), accompanied by decreased cell viability, migration capacity, and tube formation ($P < 0.05$, **Figure 6F-H**), decreased MDA level, increased SOD and GSH-Px levels ($P < 0.05$, **Figure 6I-K**), and decreased TNF-α and IL-6 levels ($P < 0.05$, **Figure 6L**, **6M**), indicating that circHIPK3 knockdown alleviated high glucose-induced cellular injury. Next, we transfected miR-125a-5p inhibitor to reduce miR-125a-5p expression and performed combination experiments with circHIPK3 knockdown ($P < 0.05$, **Figure 6B**, **6C**). In the combination group, decreased miR-125a-5p expression led to increased NDUFA5 expression ($P < 0.05$, **Figure 6D**, **6E**), along with increased cell viability, migration capacity, and tube formation ($P < 0.05$, **Figure 6F-H**), increased MDA level, decreased SOD and GSH-Px levels ($P < 0.05$, **Figure 6I-K**), and increased TNF-α and IL-6 levels ($P < 0.05$, **Figure 6L**, **6M**). These results demonstrate that circHIPK3 knockdown alleviates high glucose-induced cellular injury by upregulating miR-125a-5p.

NDUFA5 inhibition ameliorates retinal vascular pathology, oxidative stress, and inflammation in DR mice

Finally, we established a DR mouse model using STZ. Compared to the control group, the mice in the remaining three groups showed significantly decreased body weight ($P < 0.05$, **Figure 7A**) and significantly increased blood glucose ($P < 0.05$, **Figure 7B**), indicating successful model establishment. In the retina of DR mice, NDUFA5 levels were significantly increased ($P < 0.05$, **Figure 7C**, **7D**), miR-125a-5p levels were significantly decreased ($P < 0.05$, **Figure 7E**), circHIPK3 levels were significantly increased ($P < 0.05$, **Figure 7F**), oxidative stress markers (MDA increased, SOD and GSH-Px decreased) and inflammatory cytokines (TNF-α, IL-6) were elevated ($P < 0.05$, **Figure 7G-K**). In addition, the expression of pro-angiogenic factor VEGFA and endothelial cell marker CD31 was significantly up-regulated in the DR group ($P < 0.05$, **Figure 7L**). After NDUFA5 inhibition ($P < 0.05$, **Figure 7C**, **7D**), compared to the DR+sh-NC group, mice showed decreased MDA level, increased SOD and GSH-Px levels, decreased TNF-α and IL-6 levels ($P < 0.05$, **Figure 7G-K**). The expression of VEGFA and CD31 was significantly down-regulated ($P < 0.05$, **Figure 7L**). These results suggest that inhibition of NDUFA5 can improve retinal neovascularization in DR mice by regulating the expression of vascular related genes, and indirectly verify its protective effect on retinal vasculopathy.

Discussion

This study systematically investigated the expression pattern, functional role, and regulatory mechanisms of NDUFA5 in DR in bioinformatic analysis, *in vitro* cell models, and *in vivo* animal experiments. Our findings suggest a circHIPK3/miR-125a-5p/NDUFA5 regulatory relationship in DR progression, providing new mechanistic insights and potential therapeutic targets.

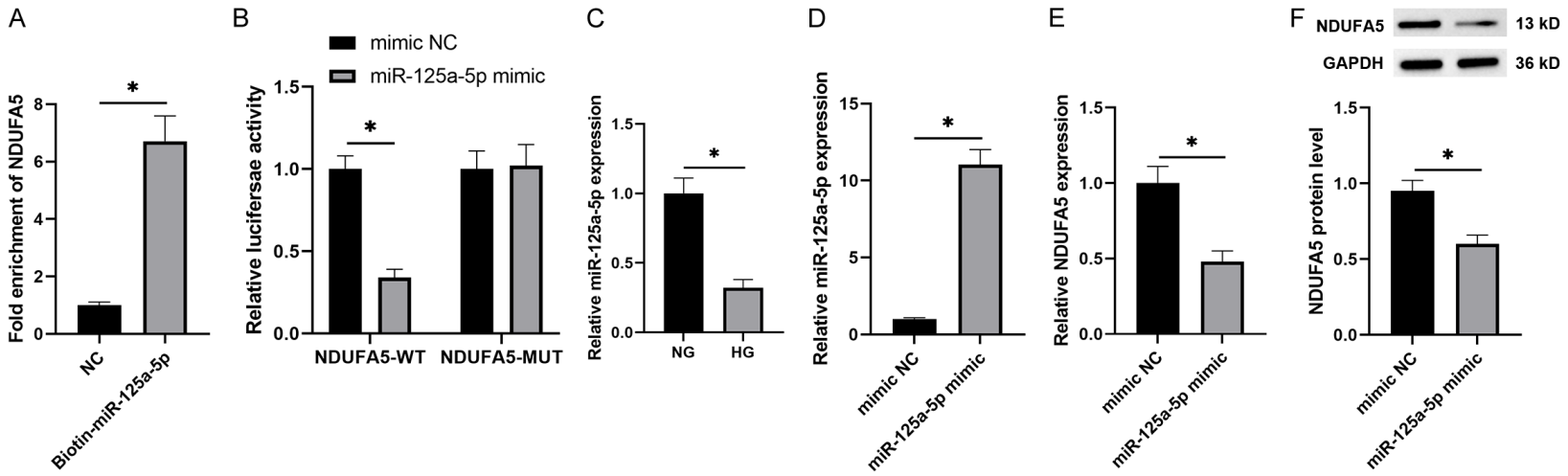

Figure 3. miR-125a-5p targets and inhibits NDUFA5 expression. A: RNA pull-down assay detecting the binding between miR-125a-5p and NDUFA5. B: Dual-luciferase reporter assay detecting binding of miR-125a-5p to the NDUFA5 3'UTR sequence. C: RT-qPCR detection of miR-125a-5p expression. hRMECs were transfected with miR-125a-5p mimic, with mimic NC as control. D: RT-qPCR detection of miR-125a-5p expression. E, F: RT-qPCR and western blot detection of NDUFA5 expression. Three independent replicates; data are mean ± SD. A, C-F: t-test. B: Two-way ANOVA with Tukey's multiple comparisons test. * indicates $P < 0.05$.

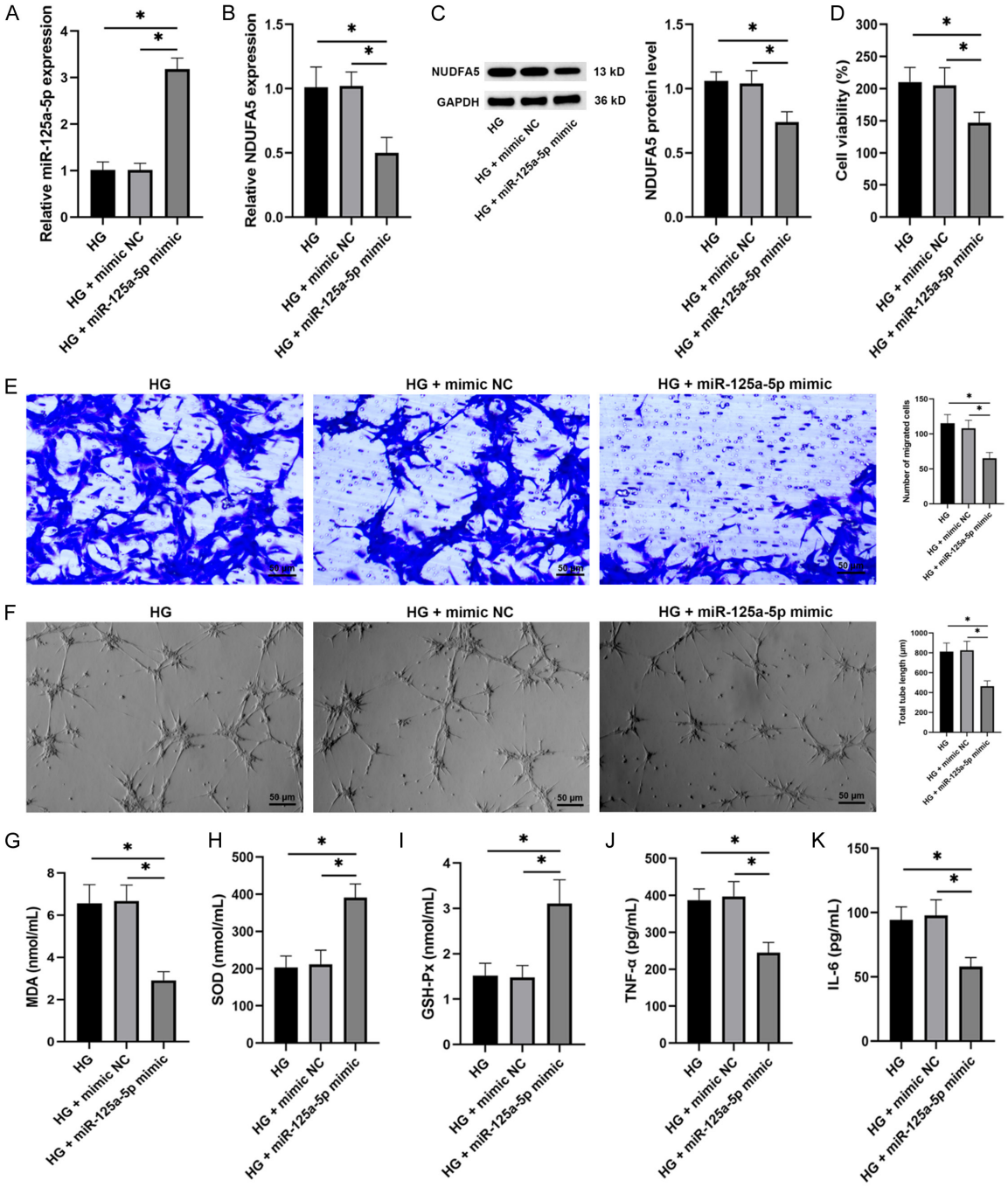

Figure 4. miR-125a-5p overexpression inhibits high glucose-induced cellular injury. HG cells were transfected with miR-125a-5p mimic, with mimic NC as control. A: RT-qPCR detection of miR-125a-5p expression. B, C: RT-qPCR and western blot detection of NDUFA5 expression. D: CCK-8 assay for cell viability. E: Transwell assay for cell migration (Scale bar = 50 μm; ×200). F: Tube formation assay for tube formation capacity (Scale bar = 50 μm; ×200). G-K: ELISA detection of oxidative stress markers (MDA, SOD, GSH-Px) and inflammatory cytokines (TNF-α, IL-6). Three independent replicates; data are mean ± SD. A-K: One-way ANOVA with Tukey's multiple comparisons test. * indicates $P < 0.05$.

The scRNA-seq data provide cell-type localization clues for NDUFA5 in rod cells, while the hRMEC experiments primarily test the role of NDUFA5 in retinal endothelial injury. These two sets of findings address different aspects of DR pathogenesis rather than representing

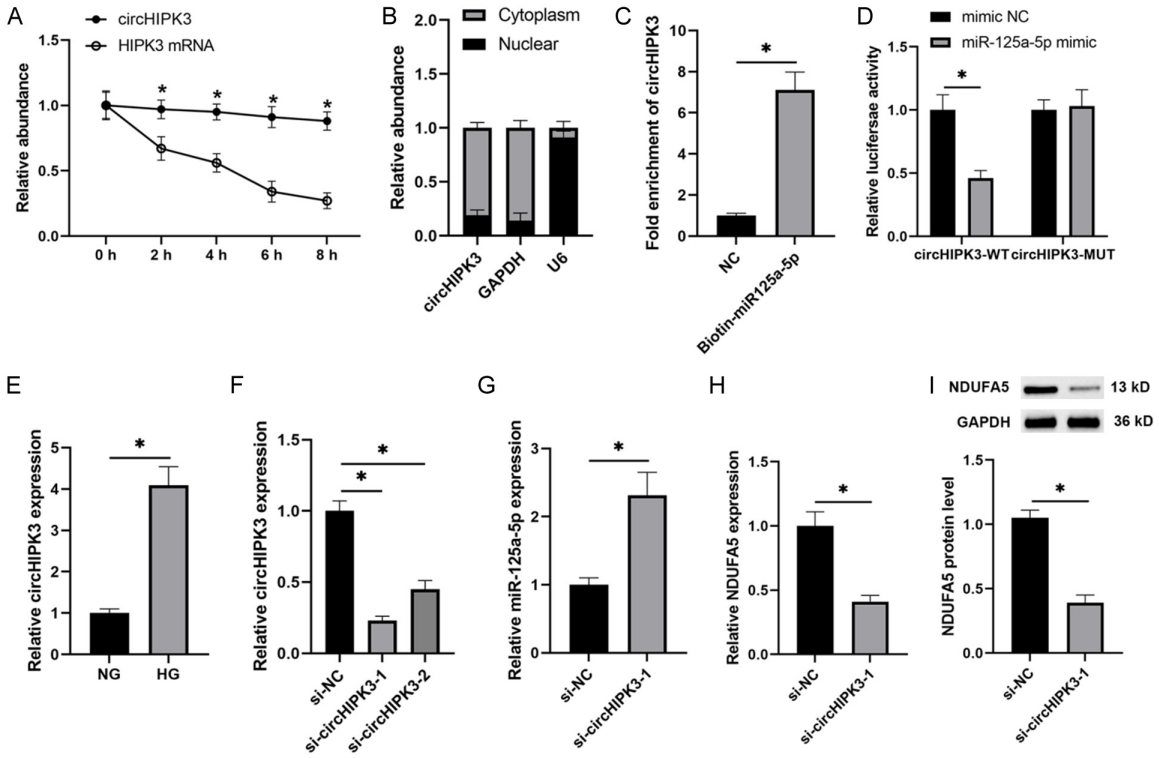

Figure 5. circHIPK3 is upregulated in HG cells and targets miR-125a-5p. A: RT-qPCR detection of circHIPK3 and HIPK3 mRNA after actinomycin D treatment. B: Nuclear-cytoplasmic fractionation for subcellular localization of circHIPK3. C: RNA pull-down assay detecting binding between circHIPK3 and miR-125a-5p. D: Dual-luciferase reporter assay detecting binding of miR-125a-5p to the circHIPK3 3'UTR sequence. E: RT-qPCR detection of circHIPK3 expression. F: hRMECs were transfected with two siRNAs targeting circHIPK3 (si-circHIPK3-1, si-circHIPK3-2), with si-NC as control. G: RT-qPCR detection of miR-125a-5p expression. H, I: RT-qPCR and western blot detection of NDUFA5 expression. Three independent replicates; data are mean ± SD. C, E, G-I: t-test. F: One-way ANOVA. A, D: two-way ANOVA with Tukey's multiple comparisons test. * indicates $P < 0.05$.

the same cell-type-specific mechanism. The scRNA-seq results revealed distinct subpopulations of rod cells in DR retinas. Rod cells were divided into three subsets: JUN+RC (normal function), Actg1+RC (development and metabolism), and NDUFA5+RC (oxidative stress-related). Statistical analysis of cell subpopulations confirmed that the oxidative stress-related NDUFA5+RC subtype was markedly increased and predominated in the retina of DR model mice. NDUFA5+RC was enriched in oxidative phosphorylation and HIF-1 signaling, consistent with role of oxidative stress in early retinal neuodegeneration in DR [5]. Rod cells are highly metabolically active and rely on heavily on mitochondrial ATP production for phototransduction [25]. As a core subunit of mitochondrial respiratory chain complex I, aberrant overexpression of NDUFA5 in rod cells may be associated with complex I dysfunction. On the one hand, decreased electron transport chain efficiency results in insufficient ATP synthesis, directly affecting rod cell phototransduction [25, 26]; on the other hand, complex I dysfunction exacerbates ROS generation, triggering oxidative stress injury [27, 28]. This is consistent with our cellular experiment results showing that NDUFA5 knockdown significantly reduced high glucose-induced MDA levels and increased SOD and GSH-Px activities, suggesting that NDUFA5 may contribute to rod cell dysfunction in early DR. Meanwhile, we identified the VEGFA+MUC subset in Müller cells, which was upregulated in the DR group and enriched in DR core pathological pathways such as VEGF and PI3K/Akt, further confirming the central role of Müller cell activation in DR vascular pathology and inflammation. More importantly, Müller cell-derived VEGFA+MUC showed enhanced PTN-SDC4 ligand-receptor communication with NDUFA5+RC. This interaction was a bioinformatic prediction and requires experi-

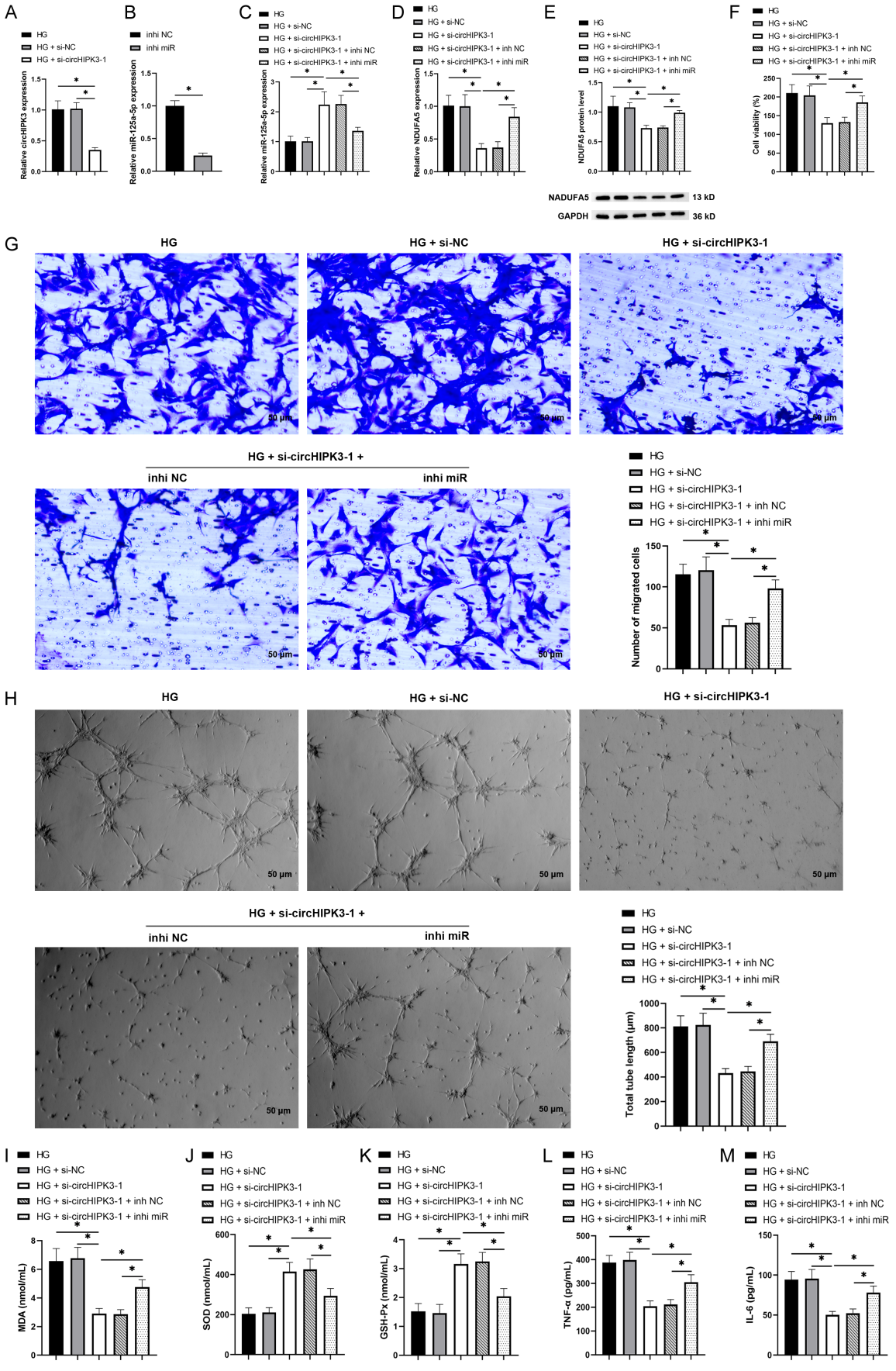
A
HG
HG + si-NC
HG + si-circHIPK3-1
Relative circHIPK3 expression
B
inhi NC
inhi miR
Relative miR-125a-5p expression
C
HG + si-circHIPK3-1 + inh NC
HG + si-circHIPK3-1 + inhi miR
Relative miR-125a-5p expression
D
Relative NDUFA5 expression
E
NDUFA5 protein level
NADUFA5
13 kD
GAPDH
36 kD
F
Cell viability (%)
G
HG + si-circHIPK3-1 +
inh NC
inhi miR
50 μm
Number of migrated cells
H
Total tube length (μm)
I
MDA (nmol/mL)
J
SOD (nmol/mL)
K
GSH-Px (nmol/mL)
L
TNF-α (pg/mL)
M
IL-6 (pg/mL)

Figure 6. circHIPK3 knockdown alleviates high glucose-induced cellular injury by upregulating miR-125a-5p. HG cells were transfected with si-circHIPK3-1, with si-NC as control. A: RT-qPCR detection of circHIPK3 expression. hRMECs were transfected with miR-125a-5p inhibitor (inhi miR), with inhibitor NC (inhi NC) as control. B: RT-qPCR detection of transfection efficiency. C: RT-qPCR detection of miR-125a-5p expression. D, E: RT-qPCR and western blot detection of NDUFA5 expression. F: CCK-8 assay for cell viability. G: Transwell assay for cell migration (Scale bar = 50 μm; ×200). H: Tube formation assay for tube formation capacity (Scale bar = 50 μm; ×200). I-M: ELISA detection of oxidative stress markers (MDA, SOD, GSH-Px) and inflammatory cytokines (TNF-α, IL-6). Three independent replicates; data are mean ± SD. B: t-test. A, C-M: one-way ANOVA with Tukey's multiple comparisons test. * indicates $P < 0.05$.

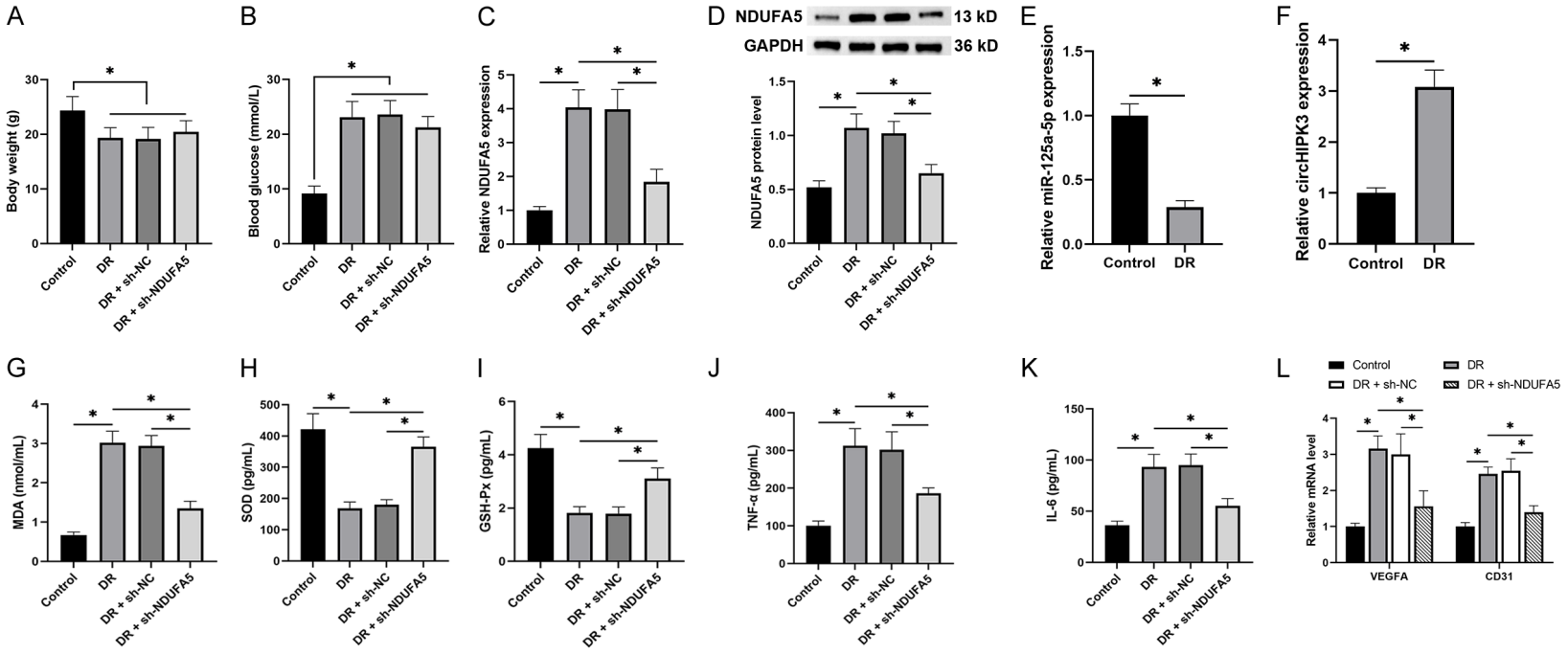

Figure 7. NDUFA5 inhibition alleviates retinal injury in DR mice. DR mouse model was established by STZ injection. DR mice received intravitreal injection of AAV-packaged sh-NDUFA5 to inhibit NDUFA5 expression, with sh-NC as control. A: Body weight. B: Blood glucose. C, D: RT-qPCR and western blot detection of NDUFA5 expression. E, F: RT-qPCR detection of miR-125a-5p and circHIPK3 expression. G-K: ELISA detection of oxidative stress markers (MDA, SOD, GSH-Px) and inflammatory cytokines (TNF-α, IL-6). L: RT-qPCR detection of VEGFA and CD31 expression. n = 6; data are mean ± SD. E, F: t-test. A-D, G-K: One-way ANOVA with Tukey's multiple comparisons test. L: Two-way ANOVA with Tukey's multiple comparisons test. * indicates $P < 0.05$.

mental validation. Previous studies have shown that the PTN-SDC4 pathway can promote disease progression by activating downstream inflammatory signals [22]. Such crosstalk may form a local inflammatory-oxidative stress loop that accelerates retinal damage. Bulk RNA-seq further verified upregulation of NDUFA5 in DR patients, supporting the clinical relevance of our findings. It is important to note that scRNA-seq analysis revealed NDUFA5 enrichment in rod cells, whereas our functional validation was performed in hRMECs, which are central to the vascular pathology of DR. This discrepancy reflects the multi-cellular nature of DR pathogenesis: NDUFA5 may exert cell-type-specific functions. Rod cells are primarily involved in early neuroretinal degeneration, while endothelial cells mediate vascular leakage and neovascularization. Given that our study focuses on vascular outcomes (oxidative stress, inflammation, tube formation), hRMECs represent a relevant model. Nevertheless, future studies will validate this axis in photoreceptor cells, retinal neurons, and retinal organoids to fully match single-cell localization data.

The ceRNA mechanism is one of the core modes by which circRNAs participate in disease regulation. circRNAs are stably expressed in the cytoplasm, possess direct binding sites for miRNAs, and regulate the expression of miRNAs and their target genes [29]. Through a series of mechanistic validation experiments, our findings suggest a potential circHIPK3/miR-125a-5p/NDUFA5 regulatory relationship. First, the actinomycin D experiment showed that circHIPK3 had a significantly longer half-life than linear HIPK3, and nuclear-cytoplasmic fractionation confirmed its predominant cytoplasmic localization, providing the structural basis for its ceRNA function. Second, RNA pull-down and dual-luciferase reporter assays directly confirmed the direct binding between circHIPK3 and miR-125a-5p, as well as between miR-125a-5p and the NDUFA5 3'UTR. Finally, functional experiments showed that under high glucose conditions, circHIPK3 and NDUFA5 were upregulated while miR-125a-5p was downregulated; circHIPK3 knockdown upregulated miR-125a-5p and downregulated NDUFA5, thereby alleviating high glucose-induced cellular injury, whereas co-transfection with miR-125a-5p inhibitor reversed this effect. To our knowledge, this study provides initial evidence linking circHIPK3 with NDUFA5, connecting the four major pathologic components of DR: circRNA regulation, oxidative stress, inflammation, and vascular injury. It also clarifies the central role of miR-125a-5p in this regulatory axis, filling a gap in the research on miR-125a-5p target genes and regulatory networks in DR. Previous studies have shown that miR-125a-5p can alleviate diabetic nephropathy by inhibiting inflammatory cytokine expression and also suppress inflammatory cytokine levels in DR [30, 31]. Our study further expands its function in DR, demonstrating that it can regulate oxidative stress, inflammation, and vascular function by targeting NDUFA5, providing new evidence for the multi-organ protective role of miR-125a-5p. The consistency between the cellular and animal experiment results provides a solid foundation for clinical translation of this study. At the cellular level, NDUFA5 knockdown or miR-125a-5p overexpression significantly alleviated high glucose-induced abnormalities in hRMEC migration, tube formation capacity, oxidative stress, and inflammation. At the animal level, intravitreal injection of AAV-sh-NDUFA5 effectively inhibited NDUFA5 expression in DR mice, significantly decreased oxidative stress and inflammation levels in retinal tissue. These results suggest that targeting NDUFA5 can improve multiple aspects of DR pathologic injury and has potential therapeutic value. The circHIPK3/miR-125a-5p/NDUFA5 regulatory axis identified in this study provides multiple potential targets for the development of novel targeted therapies for DR and is expected to enrich the treatment strategies for DR.

This study had several limitations. First, the HG cell model did not fully recapitulate the hypoxic and metabolic microenvironment in the diabetic retinopathy in humans. Second, clinical sample size was relatively small, so future studies will expand clinical cohorts and validate the axis in human vitreous samples. Third, the downstream signaling pathways of NDUFA5 remain to be fully explored. Nonetheless, our findings established the circHIPK3/miR-125a-5p/NDUFA5 axis as a novel regulator of DR and supported NDUFA5 as a promising therapeutic target.

Disclosure of conflict of interest

None.

Address correspondence to: Zhihui Zhang, Xuyong Eye Hospital, No. 26 Yongchang Road, Tiexi, Dongsheng District, Ordos 017000, Inner Mongolia, China. Tel: +86-15547754002; E-mail: Zhangzhihui319@163.com

References

[1] Aris NK and Michael WU. Diabetic retinopathy: early diagnosis and effective treatment. Dtsch Arztebl Int 2010; 107: 75-83.

[2] Mahajan N, Arora P and Sandhir R. Perturbed biochemical pathways and associated oxidative stress lead to vascular dysfunctions in diabetic retinopathy. Oxid Med Cell Longev 2019; 2019: 8458472.

[3] Li X, Dong X, Zhang W, Shi Z, Liu Z, Sa Y, Li L, Ni N and Mei Y. Multi-omics in exploring the pathophysiology of diabetic retinopathy. Front Cell Dev Biol 2024; 12: 1500474.

[4] Lei Y, Liu Q, Chen B, Wu F, Li Y, Dong X, Ma N, Wu Z, Zhu Y, Wang L, Fu Y, Liu Y, Song Y, Du M, Zhang H, Zhu J, Lyons TJ, Wang T, Hu J, Xu H, Chen M, Yan H and Wang X. Protein O-GlcNAcylation coupled to Hippo signaling drives vascular dysfunction in diabetic retinopathy. Nat Commun 2024; 15: 9334.

[5] Tang S, Huang M, Wang R, Li M, Dong N, Wu R, Chi Z and Gao L. Drp1-dependent mitochondrial fragmentation mediates photoreceptor abnormalities in type 1 diabetic retina. Exp Eye Res 2024; 242: 109860.

[6] Le D, Son T, Lim JI and Yao X. Quantitative optical coherence tomography reveals rod photoreceptor degeneration in early diabetic retinopathy. Retina 2022; 42: 1442-1449.

[7] Carpi-Santos R, de Melo Reis RA, Gomes FCA and Calaza KC. Contribution of Müller cells in the diabetic retinopathy development: focus on oxidative stress and inflammation. Antioxidants (Basel) 2022; 11: 617.

[8] Liu D, Zheng Z, Chen Z, Guo R, Weng J, Huang S and Weng S. Ferroptosis in Müller cells under hyperglycemia: mechanisms and therapeutic implications for diabetic retinopathy-associated optic neuroinflammation. Int Ophthalmol 2025; 45: 302.

[9] Li M, Peng Y, Pang L, Wang L and Li J. Single-cell RNA sequencing reveals transcriptional signatures and cell-cell communication in diabetic retinopathy. Endocr Metab Immune Disord Drug Targets 2024; 24: 1651-1663.

[10] Rak M and Rustin P. Supernumerary subunits NDUFA3, NDUFA5 and NDUFA12 are required for the formation of the extramembrane arm of human mitochondrial complex I. FEBS Lett 2014; 588: 1832-1838.

[11] Shrestha S, Wiener HW, Chowdhury S, Kajimoto H, Srinivasasainagendra V, Mamaeva OA, Brahmbhatt UN, Ledee D, Lau YR, Padilla LA, Chen JY, Dahdah N, Tiwari HK and Portman MA. Pharmacogenomics of coronary artery response to intravenous gamma globulin in kawasaki disease. NPJ Genom Med 2024; 9: 34.

[12] Nie H, Yu X, He H, Zhou L, Li Q, Song C, Wang D, Ren T, Chen Z, Huang H, Dai X and Zhou Y. Hepatocyte miR-33a mediates mitochondrial dysfunction and hepatosteatosis by suppressing NDUFA5. J Cell Mol Med 2018; 22: 6285-6293.

[13] Wang T, Li C, Shi M, Zhou S, Chen J and Wang F. Circular RNA circZNF532 facilitates angiogenesis and inflammation in diabetic retinopathy via regulating miR-1243/CARM1 axis. Diabetol Metab Syndr 2022; 14: 14.

[14] Shan K, Liu C, Liu BH, Chen X, Dong R, Liu X, Zhang YY, Liu B, Zhang SJ, Wang JJ, Zhang SH, Wu JH, Zhao C and Yan B. Circular noncoding RNA HIPK3 mediates retinal vascular dysfunction in diabetes mellitus. Circulation 2017; 136: 1629-1642.

[15] Hwang SJ, Ahn BJ, Shin MW, Song YS, Choi Y, Oh GT, Kim KW and Lee HJ. miR-125a-5p attenuates macrophage-mediated vascular dysfunction by targeting Ninjurin1. Cell Death Differ 2022; 29: 1199-1210.

[16] Liu C, Xiang J, Chen Y, He C, Tong J, Liao Y, Lei H, Sun L, Yao G and Xie Z. MiR-125a-5p in MSC-derived small extracellular vesicles alleviates Müller cells injury in diabetic retinopathy by modulating mitophagy via PTP1B pathway. Cell Death Discov 2025; 11: 226.

[17] Xu L, Li Y, Yin L, Qi Y, Sun H, Sun P, Xu M, Tang Z and Peng J. miR-125a-5p ameliorates hepatic glycolipid metabolism disorder in type 2 diabetes mellitus through targeting of STAT3. Theranostics 2018; 8: 5593-5609.

[18] Jin S, Guerrero-Juarez CF, Zhang L, Chang I, Ramos R, Kuan CH, Myung P, Plikus MV and Nie Q. Inference and analysis of cell-cell communication using CellChat. Nat Commun 2021; 12: 1088.

[19] National Research Council Committee for the Update of the Guide for the C and Use of Laboratory A. The National Academies Collection: Reports funded by National Institutes of Health. In: editors. Guide for the Care and Use of Laboratory Animals. Washington (DC): National Academies Press (US) 2011, National Academy of Sciences; 2011.

[20] Marquardt N, Feja M, Hünigen H, Plendl J, Menken L, Fink H and Bert B. Euthanasia of laboratory mice: are isoflurane and sevoflurane real alternatives to carbon dioxide? PLoS One 2018; 13: e0203793.

[21] Liang X, Brooks MJ and Swaroop A. Developmental genome-wide occupancy analysis of bZIP transcription factor NRL uncovers the role

of c-Jun in early differentiation of rod photoreceptors in the mammalian retina. Hum Mol Genet 2022; 31: 3914-3933.
[22] Sheng K, Ran Y, Feng X, Wang Y, Zhou S, Guan Y, Tan P, Qian S, Zhao Z, Zhang B, Ji W, Niu C and Guo X. PTN secreted by cardiac fibroblasts promotes myocardial fibrosis and inflammation of pressure overload-induced hypertrophic cardiomyopathy through the PTN-SDC4 pathway. Life Sci 2025; 363: 123356.
[23] Zou Q, Zhou J, Li Y, Shi J, Huang J, Zhuang C, Wu H, Hong H, Guo Y, Li Q, Zhao RC and Wang J. Lars2 deficiency-induced mitochondrial dysfunction drives the emergence of a pro-inflammatory stroke-specific microglial subpopulation. Aging Dis 2025; 17: 2213-2230.
[24] He S, Gu C, Su T and Qiu Q. Research progress of circRNAs in inflammatory mechanisms of diabetic retinopathy: an emerging star with potential therapeutic targets. Curr Eye Res 2022; 47: 165-178.
[25] Hsu SC and Molday RS. Glucose metabolism in photoreceptor outer segments. Its role in phototransduction and in NADPH-requiring reactions. J Biol Chem 1994; 269: 17954-17959.
[26] Calzia D, Panfoli I, Heinig N, Schumann U, Ader M, Traverso CE, Funk RH and Roehlecke C. Impairment of extramitochondrial oxidative phosphorylation in mouse rod outer segments by blue light irradiation. Biochimie 2016; 125: 171-178.
[27] Tretter L, Sipos I and Adam-Vizi V. Initiation of neuronal damage by complex I deficiency and oxidative stress in Parkinson's disease. Neurochem Res 2004; 29: 569-577.
[28] Lopez-Fabuel I, Le Douce J, Logan A, James AM, Bonvento G, Murphy MP, Almeida A and Bolaños JP. Complex I assembly into supercomplexes determines differential mitochondrial ROS production in neurons and astrocytes. Proc Natl Acad Sci U S A 2016; 113: 13063-13068.
[29] Misir S, Wu N and Yang BB. Specific expression and functions of circular RNAs. Cell Death Differ 2022; 29: 481-491.
[30] Hao Y, Miao J, Liu W, Cai K, Huang X and Peng L. Mesenchymal stem cell-derived exosomes carry microRNA-125a to protect against diabetic nephropathy by targeting histone deacetylase 1 and downregulating endothelin-1. Diabetes Metab Syndr Obes 2021; 14: 1405-1418.
[31] Yin R, Zhang Y, Fang X, Zhang Y, Miao R, Yao Y, Guan H and Tian J. Discovering diabetes complications-related microRNAs: meta-analyses and pathway modeling approach. BMC Med Genomics 2025; 18: 86.